Nanostructured Nb-substituted $CaMnO_3$ n-type thermoelectric material prepared in a continuous process by ultrasonic spray combustion

Sascha Populoh, Matthias Trottmann, Myriam H. Aguire, and Anke Weidenkaff[a)]
Solid State Chemistry and Catalysis, Empa, Swiss Federal Laboratories for Materials Testing and Research, CH-8600 Duebendorf, Switzerland

(Received 15 December 2010; accepted 26 April 2011)

One way to further optimize the thermoelectric properties toward a higher ZT is a temperature stable nanoengineering of materials, where the thermal conductivity is reduced by increasing the phonon scattering at the grain boundaries. To study this, Nb-substituted $CaMnO_3$ perovskite-type material was synthesized by ultrasonic spray combustion (USC). The grain growth has been characterized by x-ray diffraction, scanning electron microscopy, and transmission electron microscopy. Finally, the thermoelectric properties of compacted and sintered bulk samples from powder prepared by a continuous scalable USC process were measured up to 1050 K. The thermoelectric legs were prepared by an adapted sintering process. Here, a compromise between enhanced porosity to reduce the thermal conductivity and securing of mechanical stability and low resistivity should be obtained. Based on the grain growth mechanisms, an advanced sintering process for additional interconnection of the particles without particle growth is needed to further increase the thermoelectric performance.

I. INTRODUCTION

The expected decline of fossil-fuel resources is promoting growing interest in renewable energy technologies such as solar energy converters and waste heat recovery techniques. In manufacturing industry, automobiles, and thermal power plants, a huge amount of energy is lost as waste heat, which could be recovered and converted into electricity by a new generation of improved thermoelectric devices. This requires thermoelectric materials that are mechanically and temperature stable, nontoxic, and inexpensive. Conventional thermoelectric modules based on Bi_2Te_3[1] exhibit relatively high conversion efficiencies but limited temperature stability in air. The perovskite-type structure, $CaMn_{0.98}Nb_{0.02}O_3$ (n-type), is a promising candidate for the production of thermoelectric oxide devices. One possibility to improve the performance of the thermoelectric materials toward a higher ZT is the nanoengineering of bulk materials. Nanostructuring effects in bulk materials are a promising way to reduce the thermal conductivity κ by increasing the phonon scattering at the grain boundaries.[2] The motivation of this study is to investigate the deviation of ZT values between very promising solid state chemistry experiments and the much lower ZT values of the thermoelectric legs in the application. Prominent examples are the materials showing $ZT > 1$, which was never reproduced in a device up to now. This deviation might be caused by differences in morphology of the material due to the different production process. Nanocrystalline $CaMn_{0.98}Nb_{0.02}O_3$ was synthesized by a continuous ultrasonic spray combustion (USC) process, a low-cost, scalable, and environmentally benign method. The effect of this synthesis method suitable for large scale production on the grain growth was determined, and the results compared with powder obtained by the standard chimie douce method.[3,4] In previous studies, the method was successfully applied to produce batches of less than 1-g material.[5] Here, a systematic study of a continuous production process for thermoelectric converters is presented. The influence of different heat treatments on the phase purity and crystal size was systematically studied to find the ideal synthesis conditions for thermoelectric converter applications. Finally, the thermoelectric properties of the compressed and sintered thermoelectric legs made from USC powders are measured, and the possible improvement of ZT by a morphological variation is demonstrated.

II. EXPERIMENTAL

In the first part of the study, powders of $CaMn_{0.98}Nb_{0.02}O_3$ were synthesized batch-wise in a noncontinuous way by a chimie douce method. After the calcination at 1100 °C for 8 h, the powder was additionally ball milled for 1 h with a planetary mill (Retsch PM 400, Retsch GmbH, Haan, Germany) and grinding balls with 3-mm diameter. The milled powder was uniaxially pressed (20 kN) into round-shaped pellets ($d = 25$ mm and $h = 7$ mm). Subsequently,

a)Address all correspondence to this author.
e-mail: anke.weidenkaff@empa.ch
DOI: 10.1557/jmr.2011.140

Downloaded from https://www.cambridge.org/core. University of Basel Library, on 30 May 2017 at 18:30:33, subject to the Cambridge Core terms of use, available at https://www.cambridge.org/core/terms. https://doi.org/10.1557/jmr.2011.140

the pellets were pressed using a hydrostatic press (2000 bar). Finally, the green body was sintered at 1250 °C for 5 h. The phase purity and the crystal size were measured by x-ray diffraction (XRD) with the PANalytical X'pert pro (PANalytical, Almelo, Netherlands. This powder was used as a reference material for further studies. In the next step, the precursor solution, which is comparable to the one used for the chimie douce synthesis, was continuously pumped into the USC to be decomposed in form of an aerosol.

The synthesis parameters were adjusted to achieve a high production rate and low crystallite size to a flow of 1 L/min at a furnace temperature of 900 °C, where the solution decomposes and solid particles are formed. An additional heat treatment at 750 °C for 2 h was needed to dry the sample and remove the carbonates on the particle surface. To study the particle growth, the sintering conditions, and phase purity, a series of additional heat treatments of up to 1200 °C were performed and characterized by XRD, scanning electron microscopy (SEM) with Hitachi S-4800 (Hitachi, Tokyo, Japan), and transmission electron microscopy (TEM) with Jeol FS 2200 200 kV (Jeol Ltd., Tokyo, Japan). The different samples used in the experiments are presented in the Tables I and II.

The electrical resistivity and the Seebeck coefficient on the prepared thermoelectric legs were measured with a RZ2001i Ozawa Science measurement system (Ozawa Science Co., Nagoya, Japan). The thermal conductivity was evaluated indirectly by measurements of the thermal diffusivity (Netzsch LFA 457 Microflash, Netzsch, Selb, Germany) and the specific heat (Netzsch DSC 404 C). For the measurement of the thermal diffusivity, the surface of the sample was covered with a thin graphite layer. This coating enhances absorption of the laser beam at the surface and can prevent direct transmission of the beam through the samples. The electric and thermal transport properties were measured in the temperature range of 300 K < T < 1050 K. Finally, the thermoelectric legs were used to produce a thermoelectric oxide module (TOM).

TABLE I. Different samples prepared by chimie douce.

Sample number	Time (h)	Temperature (°C)
CD800C	6	800
CD1100C	8	1100
CDbulk1250C	4	1250

TABLE II. Different samples prepared by USC.

Sample number	Time (h)	Temperature (°C)
Starting material		
USC750C	2	750
USC750C	6	750
USC750C	12	750
USC800C	2	800
USC900C	2	900
USC1000C	2	1000
USC1100C	2	1100

III. RESULTS AND DISCUSSION

The XRD patterns reported in Fig. 1 indicate that the samples produced by the chimie douce method have to be calcined at a temperature of 1100 °C to get single phase material. Results after calcination at 800 °C reveal the occurrence of impurity phases. In contrast to this, samples produced by USC are well crystallized and phase pure after an additional heat treatment at 750 °C. For a comparison, the XRD patterns of a final bulk sintered material are also shown.

In Fig. 2, the XRD patterns for the different samples prepared by USC are shown and demonstrate the effects of the different heat treatments on the phase purity. In general, the crystallinity of all samples is good. Notably, directly after the production at 900 °C with a rate of 1 L/min, the crystallinity and the phase purity are poor. To get phase pure

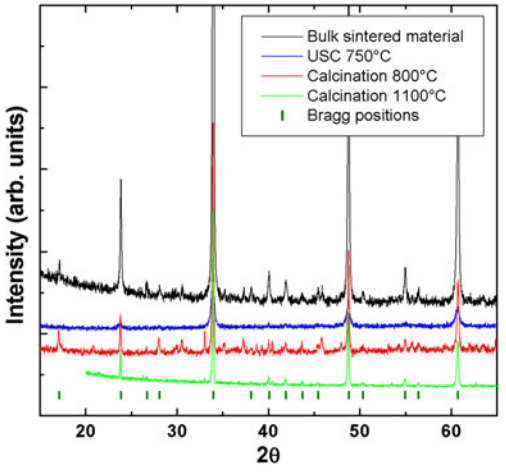

FIG. 1. X-ray diffraction (XRD) patterns of the samples produced by chimie douce.

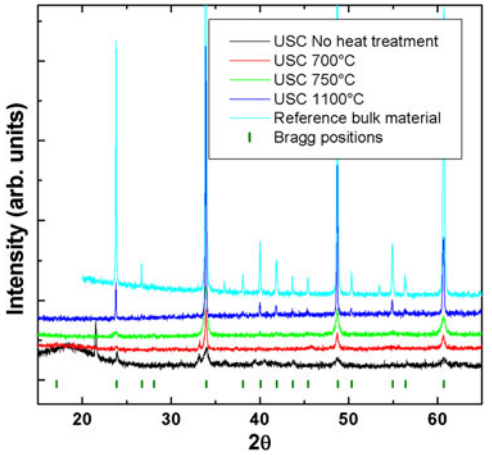

FIG. 2. XRD patterns of the samples produced by ultrasonic spray combustion (USC).

Downloaded from https://www.cambridge.org/core. University of Basel Library, on 20 Jan 2020 at 08:33:33, subject to the Cambridge Core terms of use, available at https://www.cambridge.org/core/terms. https://doi.org/10.1557/jmr.2011.140

material, additional heat treatments at different temperatures were carried out.

From these XRD patterns, the average crystal size (ACS) can be calculated using the Scherrer equation:

$$\tau = \frac{K * \lambda}{\beta \cos(\theta)} \quad ,$$

where K is the shape factor, λ is the x-ray wave length, β is the line broadening at half the maximum intensity in radians, and θ is the Bragg angle measured at the peak position around $2\theta = 34°$.[6] The results can be found in Fig. 3. A parabolic increase of the particle size can be observed when the temperature of the heat treatment is increased. At the beginning, the size of the particles prepared by USC stays nearly constant around 25–35 nm up to 800 °C. Finally, when the temperature of the heat treatment of the USC samples reaches the sintering temperature of the bulk reference sample of 1200 °C, the ACS of both specimens is similar around 500 nm.

A comparison of the powders prepared by USC and treated at 750 °C for different time spans (2–12 h) reveals an increase in the ACS of lower than 2 nm. It is important to note that this temperature is well above the maximum temperatures in which our modules are operating (cf. Ref. 7). This means that particle growth during operation in a TOM is excluded. For the phase pure sample, the ACS after the chimie douce synthesis is in the range of 250 nm. In contrast to this, for the USC samples, a phase pure compound could already be achieved with a heat treatment at 750 °C. After this, the ACS is still around 30 nm.

In a first attempt to sinter the phase pure USC powder, a pellet of 12-mm diameter was uniaxially pressed and sintered at 1100 °C for 1 h. The density of the sintered pellet was around 70% of the theoretical density, and the ACS was less than 150 nm. In comparison to the bulk sintered material (95% density), the USC-powder bulk pellet still has a three times smaller crystal size, and even the first phase pure material from soft chemistry has an ACS of 250 nm without being sintered. Nonetheless, the density of the USC powder is comparatively low, but very suitable for the thermoelectric conversion in a generator device, since the electrical conductivity is ensured by the well-interconnected small crystallites.

A previous study of the ACS by nitrogen adsorption using the Brunauer, Emmett and Teller (BET) method is showing a trend comparable with the ACS calculated using the Scherrer equation with the values from Fig. 3.

The morphology of the samples was checked by SEM and TEM as shown in Figs. 4–11. Figure 4 shows a representative SEM picture of the bulk USC powder directly after the synthesis. The diameters of the spherical agglomeration of particles are in the range of 0.5 to 5μm. In the Figs. 5–7, the particle growth with increasing heat treatment temperature could be confirmed. The significant particle growth between the samples USC750C and USC1100C is remarkable.

The TEM study was carried out on a different sample batch where the heat treatment was comparable to the one listed in Table II. The uniform formation of nanodomain

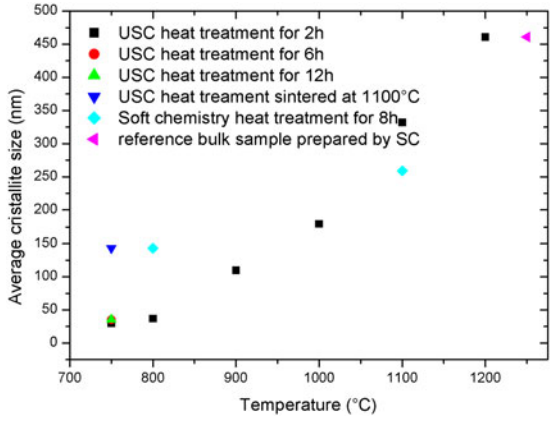

FIG. 3. Average crystal size calculated using the Scherrer equation for the different samples.

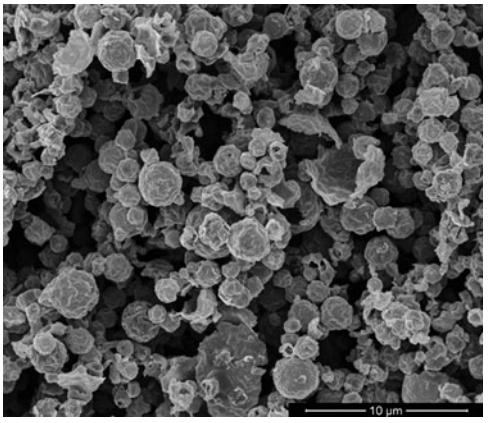

FIG. 4. Scanning electron microscopy (SEM) picture after the USC synthesis.

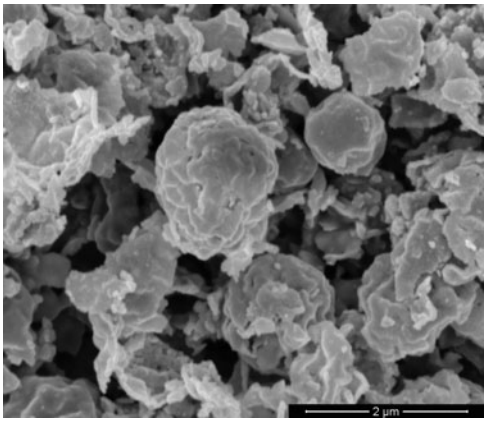

FIG. 5. SEM image after calcination at 750 °C.

Downloaded from https://www.cambridge.org/core. University of Basel Library, on 30 Nov 2017 at 08:31:15, subject to the Cambridge Core terms of use, available at https://www.cambridge.org/core/terms. https://doi.org/10.1557/jmr.2011.140

structures, for example, Ruddlesden–Popper phases, in the samples prepared by USC can be observed in Fig. 8. Such formations of domain structures within the crystallites reveal an extra nanostructuration effect and might enhance the reduction of the thermal conductivity even further. The particle size deduced from Figs. 9 and 10 is comparable to the one after the Scherrer equation as presented in Fig. 4 and shows the same trend.

Even at 1100 °C, the formation of a Ruddlesden–Popper phase is also observed, particularly in rectangular-shaped crystallites, confirming the thermodynamic stability of the nanostructuration. A high-resolution TEM micrograph of this phase is presented in Fig. 11. The disorder caused by this Ruddlesden–Popper phase is another mechanism limiting the thermal conductivity in our compound similar to the twinned domains observed by Bocher et al.[8,9]

For the determination of the thermoelectric properties, a bulk sample was produced from the USC powder as described above. These additional heat treatments are clearly contradictory to the advantages of the USC powder but necessary for the low-cost production of thermoelectric legs for high-temperature converters. Only well-sintered materials ensure a thermomechanical stability of the

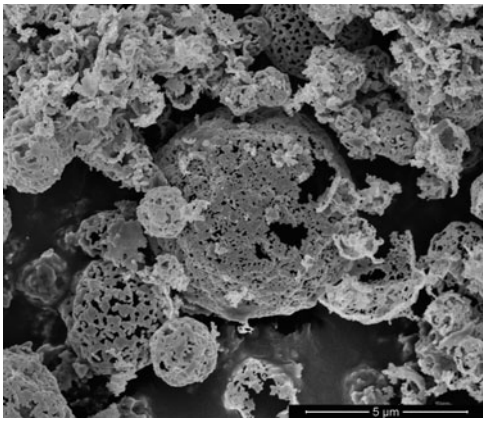

FIG. 6. SEM image after calcination at 900 °C.

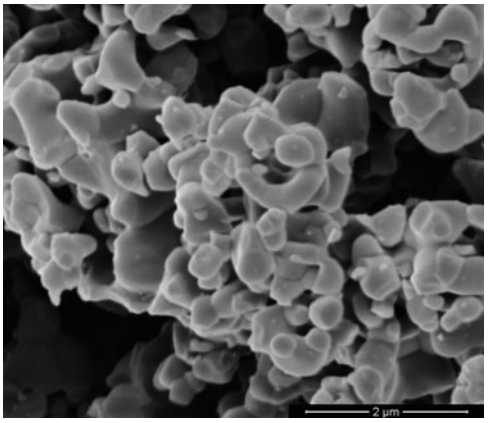

FIG. 7. SEM image after calcination at 1100 °C.

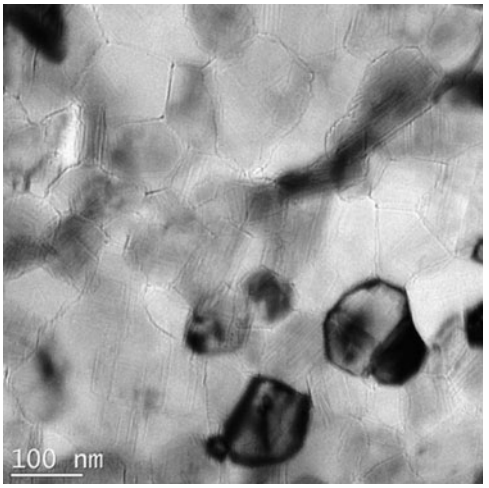

FIG. 8. Transmission electron microscopy (TEM) image of a typical sphere wall in a sample prepared by USC.

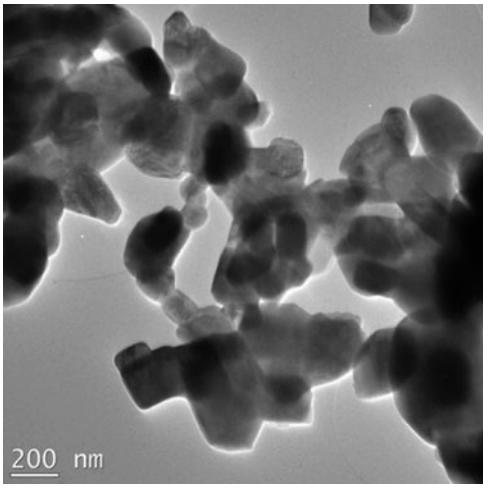

FIG. 9. TEM image of the sample USC1000C.

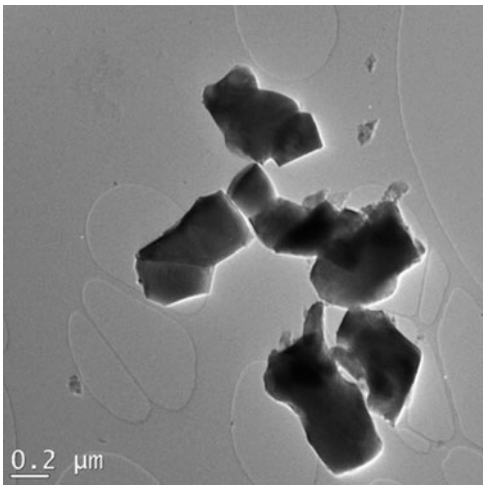

FIG. 10. TEM image of the sample USC1100C.

Downloaded from https://www.cambridge.org/core. University of Basel Library, on 30 May 2017 at 13:33:33, subject to the Cambridge Core terms of use, available at https://www.cambridge.org/core/terms. https://doi.org/10.1557/jmr.2011.140

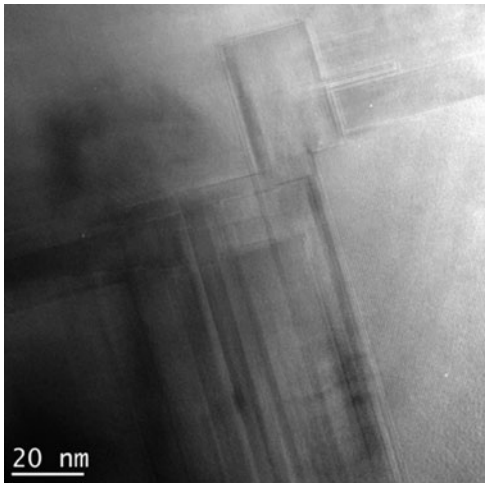

FIG. 11. Zoomed-in TEM image of the sample USC1100C.

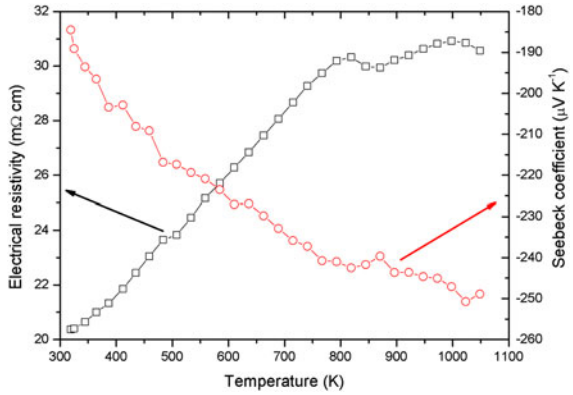

FIG. 12. Electrical conductivity and Seebeck coefficient against temperature.

sintered bodies, and a good interconnection of the grains is required for good bulk-transport properties.

In Fig. 12, the Seebeck coefficient and the electrical resistivity of the above described sample are presented. The resistivity increases from around 20 mΩ·cm at room temperature to 31 mΩ·cm at 1050 K, while also the value of the Seebeck coefficient increases from −180 to −250 $\mu V \cdot K^{-1}$. This behavior corresponds to the values reported for the performing manganate legs in TOMs,[10] where the relative density of the sintered pellet was around 20% higher. This is a proof that the enhanced porosity is acceptable for the application to substantially reduce the thermal conductivity term. In Fig. 13, the behavior of the thermal conductivity in the same temperature range can be found. It has to be noted that the measurement of the thermal diffusivity of porous materials requires to take special care (as mentioned above) but gives adequate values down to porosities of 50% as shown in Refs. 7 and 11. Due to the different morphology, that is, smaller particle size of the samples sintered from USC powder, it is expected that the lattice part of the thermal conductivity

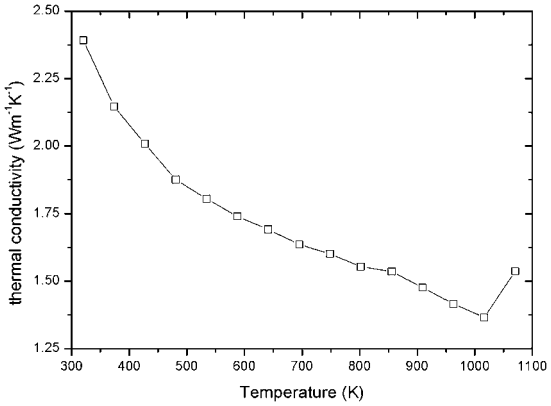

FIG. 13. Thermal conductivity between room temperature and 1050 K.

is reduced. The thermal conductivity decreases from the room temperature value of approximately 2.5 $W \cdot m^{-1} \cdot K^{-1}$ to less than 1.5 $W \cdot m^{-1} \cdot K^{-1}$ above 1000 K. In comparison to the reported values,[10] the thermal conductivity for the application-ready sintered bodies is about 20% lowered. In porous materials, the thermal conductivity is lowered compared with the dense material. From the measurement of a porous material, it is under several assumptions (spherical, well-separated pores) possible to calculate the thermal conductivity of a dense material with the help of the Maxwell equation.[12] In a thermoelectric leg, it is acceptable to have porous materials to reduce the thermal conductivity as long as a good electrical conductivity is preserved and the thermomechanical stability is high enough.

In total, this results in a maximum ZT value of 0.15 at around 1000 K. In summary, our samples with a lower relative density showed the same electrical conductivity in combination with a lowered thermal conductivity, which leads to comparison with the ZT value given in Ref. 10 at 800 K, showing that our value is with 0.1 around 20% higher than the previously reported. This reveals an increase in the overall thermoelectric performance of the material. Furthermore, this increase in the performance is conserved in long-term operation in thermoelectric modules.

IV. CONCLUSIONS

The crystal size of the powder after the calcination was successfully decreased by using the USC technique. This method allows applying a lower temperature of the heat treatment needed to obtain a pure phase compared with other synthesis methods. The first sintering experiment with a uniaxially pressed green body using the USC powder led to promising density values combined with a small crystal size. The existence of the formation of a Ruddlesden–Popper phase in the crystal structure up to 1100 °C is remarkable because it might be a stable form of nanostructuration to disturb the phonon transport. To quantify the influence of the Ruddlesden–Popper phase formation,

Downloaded from https://www.cambridge.org/core. University of Basel Library, on 30 Nov 2016 at 08:31:15, subject to the Cambridge Core terms of use, available at https://www.cambridge.org/core/terms. https://doi.org/10.1557/jmr.2011.140

further more detailed studies are planned. Finally, the material prepared from USC powder showed an increased thermoelectric performance. For long-term, high-temperature applications, for example, in a solar thermoelectric converter, the reduced density of the sintered USC material has to be tested. A follow-up study using the USC powder and spark plasma sintering to suppress the crystal growth and meanwhile to increase the density is in progress. This is especially interesting as the lower ACS of the USC powder is still conserved in the samples sintered at 1100 °C and three times smaller than the samples obtained from chimie douce. An improved sintering at lower temperatures and/or shorter times would enhance the benefit from the fact that via USC, phase pure powder is obtained at much lower temperatures even more, while an increased density would also lead to a higher electrical conductivity.

ACKNOWLEDGMENTS

The authors acknowledge Nico Studer for the great work on the USC, Songhak Yoon for help in the XRD measurements, Oliver Brunko for the help in sample preparation, Ye Lu for the BET experiments, Lassi Karvonen for help and discussion about the heat treatment of the samples, and finally Petr Tomeš for help with the data treatment.

REFERENCES

1. S.S. Kim, F. Yin, and Y. Kagawa: Thermoelectricity for crystallographic anisotropy controlled Bi–Te based alloys and p–n modules. *J. Alloy. Comp.* **419**, 306 (2006).
2. P. Pichanusakorn and P. Bandaru: Nanostructured thermoelectrics. *Mater. Sci. Eng., R* **67**, 19 (2010).
3. A. Weidenkaff: Preparation and application of nanostructured perovskite phases. *Adv. Eng. Mater.* **6**, 709 (2004).
4. E. Krupicka, A. Reller, and A. Weidenkaff: Morphology of nanoscaled LaMO3-particles (M=Mn, Fe, Co, Ni) derived by citrate precursors in aqueous and alcoholic solvents. *Cryst. Eng.* **5**, 195 (2002).
5. L. Bocher, R. Robert, M.H. Aguirre, S. Malo, S. Hébert, A. Maignan, and A. Weidenkaff: Thermoelectric and magnetic properties of perovskite-type manganate phases synthesised by a ultrasonic spray combustion (USC). *J. Sol. State Sci.* **10**, 496 (2008).
6. A.L. Patterson: The Scherrer formula for x-ray particle size determination. *Phys. Rev.* **56**, 978 (1939).
7. J. Blumm: Thermophysical properties characterization of zirconia prior to, during and after the sintering process. *CFI-Ceram. Forum Int.* **82**, E32 (2005).
8. L. Bocher, M.H. Aguirre, R. Robert, D. Logvinovich, S. Bakardjieva, J. Hejtmanek, and A. Weidenkaff: High-temperature stability, structure and thermoelectric properties of $CaMn_{1-x}Nb_xO_3$ phases. *Acta Mater.* **57**, 5667 (2009).
9. L. Bocher, M.H. Aguirre, D. Logvinovich, A. Shkabko, M. Trottmann, and A. Weidenkaff: $CaMn_xNb_{1-x}O_3$ perovskite-type phases as promising new high temperature thermoelectric materials. *Inorg. Chem.* **47**, 8077 (2008).
10. P. Tomeš, M. Trottmann, C. Suter, M.H. Aguirre, A. Steinfeld, P. Haueter, and A. Weidenkaff: Thermoelectric oxide modules (TOMs) for the direct conversion of simulated solar radiation into electrical energy. *Materials* **3**, 2801 (2010).
11. X. Song, M. Xie, F. Zhou, G. Jia, X. Hao, and S. An: High-temperature thermal properties of yttria fully stabilized zirconia ceramics. *J. Rare Earths* **29**, 155 (2011).
12. K.W. Schlichting, N.P. Padture, and P.G. Klemens: Thermal conductivity of dense and porous yttria-stabilized zirconia. *J. Mater. Sci.* **36**, 3003 (2001).

Downloaded from https://www.cambridge.org/core. University of Basel Library, on 30 May 2017 at 08:33:33, subject to the Cambridge Core terms of use, available at https://www.cambridge.org/core/terms. https://doi.org/10.1557/jmr.2011.140